Correspondence and requests for materials should be addressed to A.B.E. (a.b.evlyukhin@ daad-alumni.de)

OPEN

Optical spectroscopy of single Si nanocylinders with magnetic and electric resonances

Andrey B. Evlyukhin[1], René L. Eriksen[2], Wei Cheng[1], Jonas Beermann[2], Carsten Reinhardt[1], Alexander Petrov[3], Stefan Prorok[3], Manfred Eich[3], Boris N. Chichkov[1] & Sergey I. Bozhevolnyi[2]

[1]Laser Zentrum Hannover e.V., Hollerithallee 8, D-30419 Hannover, Germany, [2]Department of Technology and Innovation, University of Southern Denmark, Niels Bohrs Allé 1, DK-5230 Odense M, Denmark, [3]Institute of Optical and Electronic Materials, Hamburg University of Technology, Eissendorfer Str. 38, D-21073 Hamburg, Germany.

Resonant electromagnetic properties of nanoparticles fabricated from high-index semiconductor or dielectric materials are very promising for the realization of novel nanoantennas and metamaterials. In this paper we study optical resonances of Si nanocylinders located on a silica substrate. Multipole analysis of the experimental scattering spectra, based on the decomposed discrete dipole approximation, confirms resonant excitation of electric and magnetic dipole modes in the Si nanocylinders. Influences of light polarization and incident angle on the scattering properties of the nanocylinders are studied. It is shown that the dependence of resonant excitation of the electric and magnetic modes in the nanocylinders on incident angle and polarization of light allows controlling and manipulating the scattered light in this system. The demonstrated properties of Si nanocylinders can be used for the realization of dielectric metasurfaces with different functional optical properties.

It is well-known from Mie theory that the first and second lowest resonances of dielectric particles correspond to the magnetic and electric dipole terms[1]. For higher refractive indexes, the quality factors of these Mie resonances and their light scattering efficiency increase. Due to these properties, the high-refractive index dielectric particles are considered as promising building blocks for the creation of metamaterials with negative effective permeability and permittivity[2]. Experimental demonstrations of dielectric metamaterials with strong magnetic and electric responses at microwave and mid-infrared frequencies were reported[2,3]. Recently, strong magnetic and electric dipole resonant responses of silicon spherical nanoparticles were predicted theoretically in the visible spectral range[4] and in the infrared region[5,6], and have been demonstrated experimentally[7–9]. Using these optical properties of Si nanoparticles new all-dielectric optical nanoantennas[10–12] and optical metamaterials[5,9,13,14] have been suggested. Recently, it has been theoretically[15] and experimentally[16] shown that the spectral positions of electric and magnetic dipole resonances of Si nanoparticles can be tuned by changing their shape. For example, it is possible to excite electric and magnetic dipole resonances at the same optical frequency for Si nanodisks by changing their aspect ratio[15,16]. This possibility allows controlling light scattering charcteristics by using Si nanodisks or nanocylinders with definite size parameters. This is one of the reasons why optical properties of cylindrical-shaped dielectric nanoparticles has been intensively studied recently[16–20]. It was experimentally demonstrated that a two-dimensional periodic array of silicon nanocylinders fabricated on a substrate and supporting Mie resonances yields almost zero total reflectance over the all visible spectral range[17]. Optical resonances of cylindrical Si nanoparticles located on different substrates and irradiated by normally incident light waves have been considered theoretically[18]. The influence of Mie resonances on the light absorption in periodic Si nanocylinders arrays has been experimentally demonstrated and studied in Ref. 20. In this paper, we investigate experimentally and theoretically optical resonant properties of single cylindrical Si nanoparticles located on a silica substrate and discuss the role played by excited multipole modes in their extinction and scattering spectra. Influences of light polarization and incident angle on the scattering diagram are studied as well.

Results

Experiment. Scanning electron microscope (SEM) images of fabricated Si nanocylinders located on a silica substrate are shown in Fig. 1. The height of all nanocylinders is determined by the thickness of Si layer on a
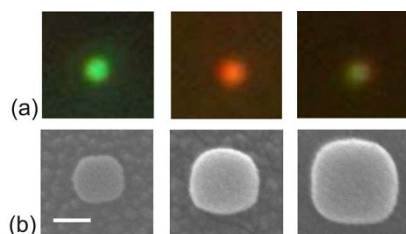
Figure 1 | (a) Dark-field images of cylindrical Si nanocylinders with diameters of ≈109, ≈143, ≈203 nm (from the left to the right) on a silica substrate. (b) Corresponding top view SEM images of the nanoparticles and substrate. To improve contrast in SEM images the nanocylinders were covered by a thin gold layer (≈15 nm) subsequent to dark-field measurements. The scale bar presents 100 nm and refers to all images in (b).

Soitec SOI wafer (Fig. 9a) and is equal to 220 nm. Their diameters vary in the range of 109 to 203 nm. In order to increase the contrast of SEM images, Si nanocylinders were covered by a thin gold layer after measurements of their optical spectra. Corresponding SEM images of the Si nanocylinders with the gold covering are shown in Fig. 1b. Dark-field images of the Si nanocylinders are presented in Fig. 1a. Different colors are produced by nanocylinders with different diameters indicating a strong dependence of scattering resonances on this parameter. Note that for nanocylinders with small diameters (109 nm and 143 nm) the dark-field images are homogeneous in color, whereas for the nanocylinder with diameter 203 nm the dark-field image has different colors. As it will be shown below, in the first case the dark-field images are determined by the resonantly excited dipole modes, in the second case the image is formed by several resonantly excited high-order modes at different wavelengths.

In order to consider this effect in more details, we performed single nanoparticle spectroscopy measurements and corresponding numerical simulations. Figure 2 demonstrates the experimental back-scattering spectra of Si nanocylinders with different diameters. It is clear that all scattering spectra have several resonant peaks, which spectral positions depend on the particle diameters. The main (maximal) resonant peaks are red shifted with the increasing particle diameter. However, for the largest particle the main peak is in the near infrared and hence the particle visually appears due to higher order modes (Fig. 1a). The width and magnitude of the resonant peaks are also increasing with the growth of the diameters. Note that for the relatively big nanocylinder (diameter of 203 nm) in Fig. 2a there are several resonant peaks, whereas for nanocylinders with small diameters there is only single resonant peak (Fig. 2b).

Calculated spectra. It is known that Si cylindrical nanoparticles can support optical resonances of both electric and magnetic types[15,17,18,21]. Spectral positions of the resonances are dependent on the particle aspect ratio and incident-light direction and polarization. In order to clarify the role of Si-nanocylinder magnetic and electric modes in the resonances presented in Fig. 2 we calculated scattering cross-sections for Si nanocylinders using the method of decomposed discrete dipole approximation (DDDA). In our simulations we consider a single Si nanocylinder irradiated by linear-polarized plane wave which obliquely falls on a substrate with refractive index of 1.5 (Fig. 3), incident angle is chosen to be 70 degrees. Because in the experiment the incident light illuminates the sample from all sides the light polarization condition is not totally defined. Therefore, we shall consider interaction of scatterers with incident light waves of *TM* (the magnetic field of incident light is perpendicular to the *XZ*-plane in Fig. 3) and *TE* (the electric field of incident light is perpendicular to the *XZ*-plane in Fig. 3) polarizations. Dielectric permittivity for crystalline Si is taken from
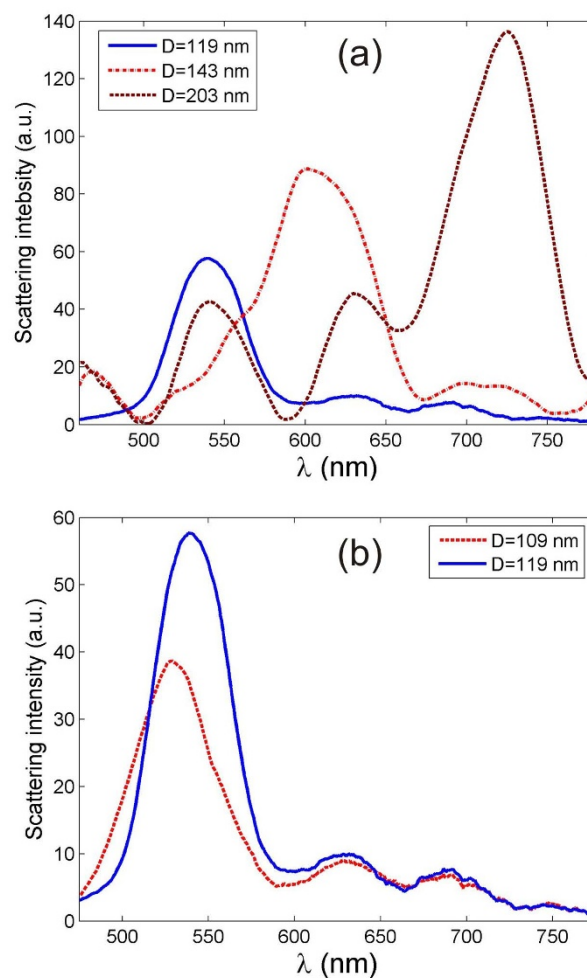

Figure 2 | **Experimental back-scattering spectra of cylindrical Si nanoparticles with diameters D.** The particle heights are 220 nm.

Ref. 22. Optical spectra of scattering cross-sections calculated for Si nanocylinders with different diameters are presented in Fig. 4. Independent on light polarization, the resonant peaks are shifted to the red side with increasing nanocylinder diameters (Fig. 4a, b). The spectral behavior of the scattered cross-sections in Fig. 4 agrees
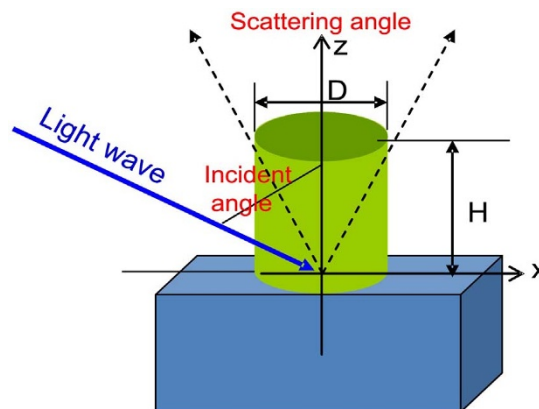

Figure 3 | **Schematic representation of the physical system involved in the numerical simulations:** a cylindrical particle (height *H* and diameter *D*) placed on a glass substrate is illuminated by a light wave, only scattered waves propagating into the scattering angle-region give contributions into calculated scattering cross-sections.

with experimental curves presented in Fig. 2 indicating the adequacy of the theoretical model. The spectral positions of resonances are also independent on light polarization. For example, for the nanocylinder with $D = 150$ nm the main difference between the first resonances shown in Figs. 4a and 4b is only in relative values of its two shoulders (in the *TE* polarization case the second shoulder at $\lambda = 675$ nm is more noticeable than in the case *TM* polarization). Such tendency is conserved for the nanocylinders with smaller diameters. However, for the nanocylinder with diameter $D = 90$ nm this difference is considerably reduced (Fig. 4c) and the scattering cross-sections agree with experimental spectra presented in Fig. 2b. In spite of qualitative agreement between the experimental spectra in Fig. 2 and theoretical data in Figs. 4, there are noticeable differences. The diameters of nanocylinders in our experiment are larger than that in simulations. due to a small oxide shell created on Si nanoparticles during the fabrication process. Thus the effective size of the Si nanoparticle, which determines the resonance position in the experiment, decreases[7].

In order to clarify the origins of the main resonant peaks in Fig. 4 we applied the multipole decomposition[15,21] to the scattering electric fields and compared the scattering cross-sections, calculated separately for different multipole moments of a nanocylinder, with general scattering cross-section. In our simulations we calculated the multipole moments of the nanocylinder with respect to its center of mass. Results of this comparison are shown in Fig. 5 for the Si nanocylinder with diameter of 100 nm. The first low-frequency resonance (wavelength $\lambda = 590$ nm) corresponds to the excitation of the magnetic dipole (MD) moment of the nanocylinder independently of light polarization. The shoulder in Fig. 5a and the peak Fig. 5b at same $\lambda = 540$ nm are basically determined by the electric dipole (ED) moment of the nanocylinder. In the case of *TE*-polarization the MD scattering cross-section has two resonant peaks corresponding to resonant excitation of the in-plane component ($\lambda = 590$ nm) and out-of-plane component ($\lambda = 520$ nm) of the nanocylinder's MD. Note that a magnetic quadrupole (MQ) resonance appears on the background of broad ED and MD resonances for both polarizations. Its influence on the calculated scattering spectra is relatively weak. Differences between positions of the resonant peaks of the total scattering cross-sections and the multipole scattering cross-sections in Fig. 5 are explained by contributions of the interference between multipole fields into the total scattering cross-sections calculated for the scattering angle 80° as shown in Fig. 3.

Regardless of a certain similarity between the scattering cross-sections for different light polarizations presented in Fig. 4 there are important differences with respect to multipole excitations. Under inclined light incidence at a large incident angle the main dipole components excited by light are out-of-plane (z-) component of ED and in-plane (x-) component of MD for the *TM* polarization and vice-versa for the *TE* polarization. Because the out-of-plane dipoles do not radiate light normally to substrate surface, the scattering cross-section into the relatively small scattering angle (Fig. 3 and Fig. 4) is basically determined by the in-plane components of ED and MD. As a result we see similarities between corresponding scattering cross-sections presented in Figs. 4a and 4b. This situation is significantly changed if total extinction and full (into all directions) scattering cross-sections are considered. From Fig. 6 one can see that the values of the extinction and scattering cross-sections in the *TE*-polarization case are much smaller than for the *TM*-polarization. In the latter case the main (out-of-plane) component of ED moment and the only (in-plane) component of MD moment are resonantly excited by light at the same wavelength region increasing the extinction and scattering (Fig. 6a). In the case of *TE* polarization the resonances of the main (out-of-plane) component ($\lambda = 520$ nm) and in-plane component ($\lambda = 590$ nm) of MD moment resonance are realized outside of the ED resonance (Fig. 6b). Moreover the con-
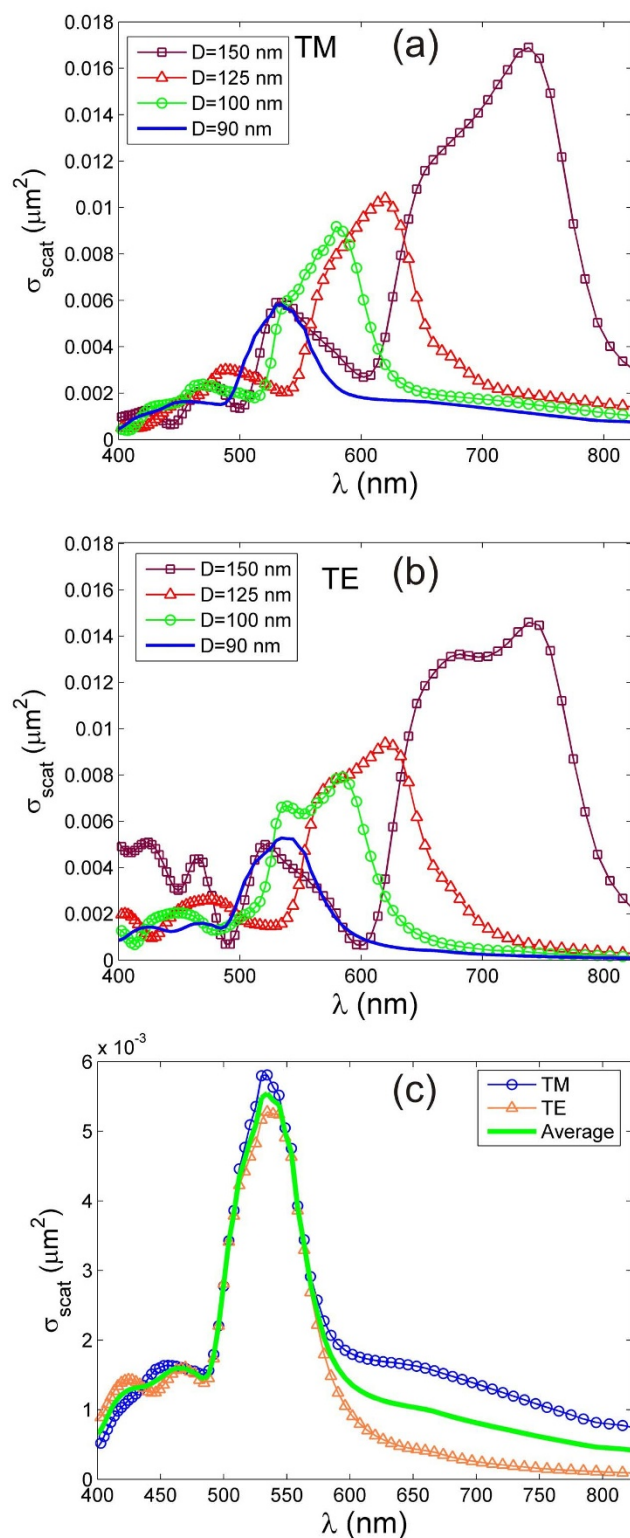

Figure 4 | **Calculated spectra of scattering cross-sections into the conical region with scattering angle 80 degrees (Fig. 3) of Si nanocylinders.** (a) Scattering of *TM*-polarized light plane waves. (b) Scattering of *TE*-polarized light plane waves. (c) Scattering cross sections (SCS) of Si nanocylinder with diameter $D = 90$ nm calculated for *TM*- and *TE*-polarized incident light, the green curve was calculated for polarization averaging. The height of the all nanocylinders is equal to 220 nm, the incident angle is equal to 70 degrees. λ is the wavelength of the incident light.
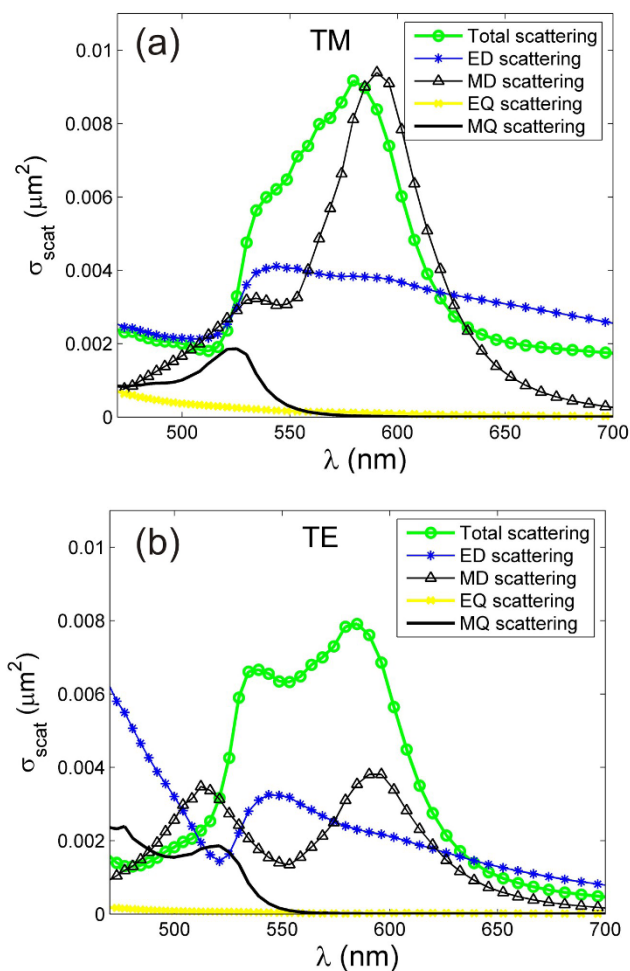
Figure 5 | Calculated spectra of total scattering cross-sections into the conical region with scattering angle 80 degrees (Fig. 3) of a Si nanocylinder irradiated by light waves of (a) *TM* **polarization and (b)** *TE* **polarization. The nanocylinder diameter is equal to 100 nm.** Other parameters are presented in Fig. 4. The scattering cross sections calculated separately for different multipole moments of nanocylinder are also presented: ED - electric dipole; MD - magnetic dipole; EQ - electric quadrupole; MQ - magnetic quadrupole.

tributions of the in-plane ED component into the extinction and scattering cross-sections in Fig. 6b are much smaller than the contributions of the out-of-plane ED component in Fig. 6a due to differences between corresponding components of the ED polarizability tensor of cylindrical nanoparticles. Comparing the extinction and scattering cross-sections in Fig. 6 one can see that the relative light absorption is weaker for *TM* polarization.

Influence of the incident angle. The extinction cross-sections of the Si nanocylinder in Fig. 5 calculated as a function of the incident angle and the wavelength are demonstrated in Fig. 7 for the two polarizations. It can be seen that for small incident angles (from 0 to 30 degrees) the extinction spectra are very similar for both polarizations. The main resonances excited by light with wavelengths of 520 nm and 590 nm correspond to the inplane electric and in-plane magnetic dipole moments of the nanocylinder, respectively. For incident angles larger than 30 degrees there are principal differences. For *TM*-polarized light the cross-section at $\lambda = 590$ nm starts to increase achieving the maximum around the incident angle of 60 degrees (Fig. 7a). This effect is explained by the increase of both out-of-plane electric dipole and in-plane magnetic dipole moments of the scatterer. Note that the resonant wavelengths of these two dipole
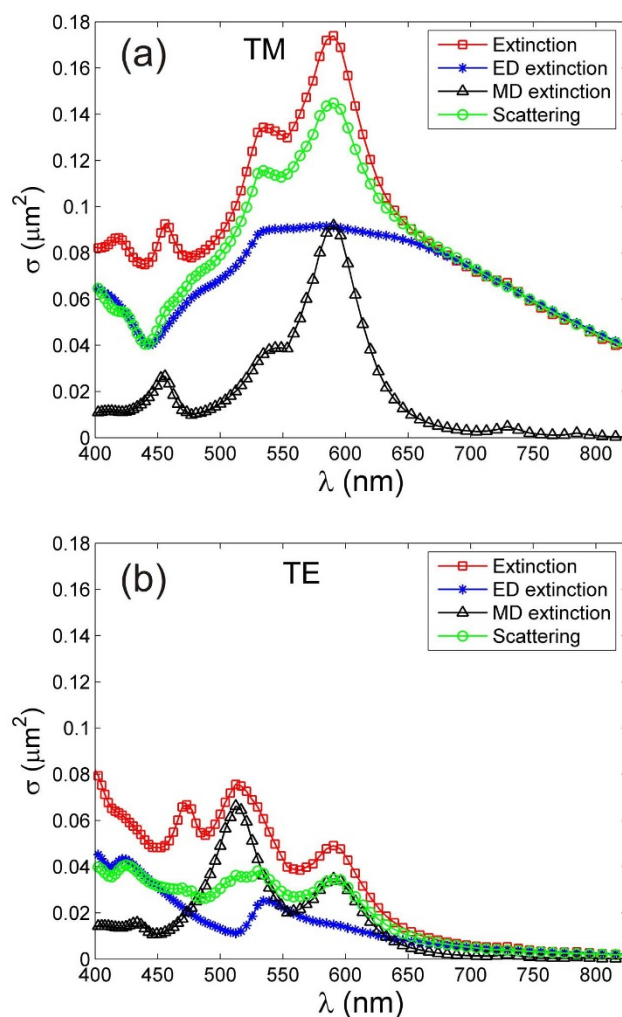

Figure 6 | Calculated spectra of total extinction and scattering cross-sections of a Si nanocylinder irradiated by light waves of (a) *TM* **polarization and (b)** *TE* **polarization. The nanocylinder diameter is equal to 100 nm.** Other parameters are presented in Fig. 4. Contributions of the nanocylinder electric dipole (ED) and magnetic dipole (MD) moments into the extinction cross-sections are also presented.

modes coincide, but the out-of-plane electric dipole resonance is significantly broader than the magnetic dipole resonance (Fig. 6a). For incident angles larger than 75 degrees all resonances become weak due to strong decreasing of total incident electric and magnetic fields (in this angle region the reflection coefficients approach to -1 for both polarizations, therefore the total external electric and magnetic fields approach zero)[23]. In contrast, in the case of *TE* polarization (Fig. 6b) the resonant values of the extinction (scattering) cross-sections decrease with increasing incident angle.

Dependence of resonant excitation of the electric and magnetic dipole modes in the nanocylinders on incident angle and polarization of light allows controlling and shaping the scattered light in the system. Figure 8 demonstrates the possibility to change the light scattering pattern by changing polarization under a fixed incident angle. For *TM* polarization there is a strong asymmetric scattering into the substrate (Fig. 8a) due to interference between the fields generated (scattered) by the resonantly excited out-of-plane electric and in-plane magnetic dipole moments of the Si nanocylinder. It presents Kerker's type scattering[24–26] for Si nanocylinders located on a glass substrate. In the conditions of *TM*-polarization, for large incident angles, we have a situation that is qualitatively similar to the case when a Si nanodisk is irradiated normally by linear polarized
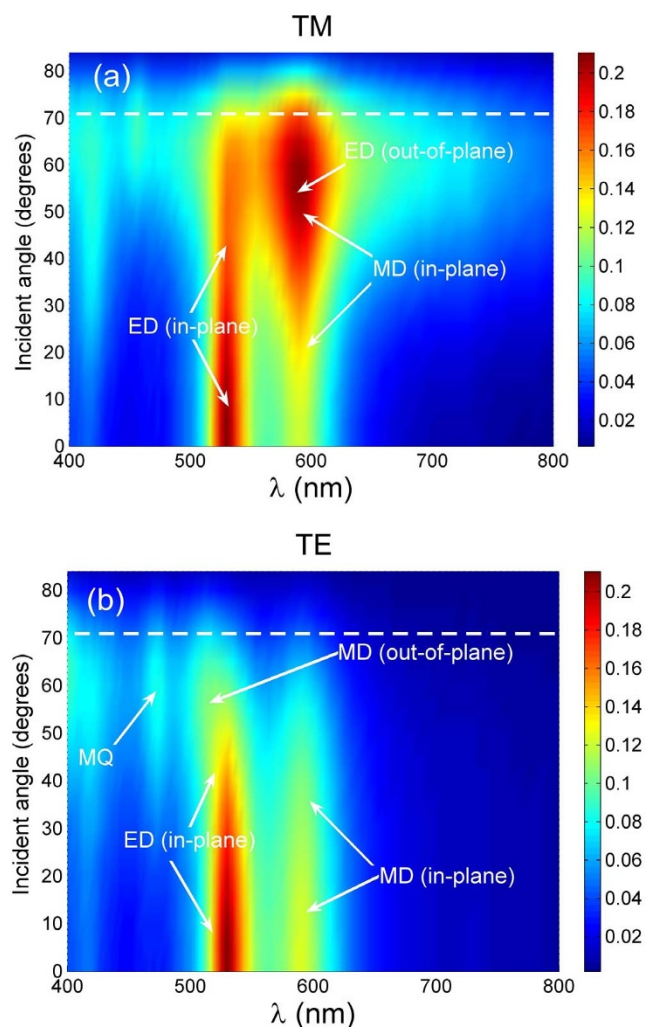
Figure 7 | Extinction cross-sections (μm²) of Si nanocylinders from Fig. 5 (height is 220 nm, diameter is 100 nm) calculated as a function of the incident angle and the wavelength for (a) *TM*-polarized and (b) *TE*-polarized incident light. Arrows in (a) show the dipole modes which give the main contributions into the extinction cross-sections. Dashed lines correspond to the extinction spectra presented in Fig. 6. Arrows indicate the resonant contributions of corresponding multipole moments.

light[16]. In these conditions the electric and magnetic dipole resonances can be excited at the same spectral region (like it is shown in Fig. 6a) resulting in the highly directive scattering pattern[16] due to interference between the electric-dipole and magnetic-dipole scattered fields[24]. Note that similar asymmetrical distrubution of electromagnetic field can be observed in the system of two metal nanoparticles with detuned electric-dipole responses[27]. Symmetrical scattering pattern in case of *TE* polarization (Fig. 8b) is determined by the in-plane component of the magnetic dipole moment. Black regions outside the white dash circles in Fig. 8, for $\theta > \pi/2$, are the forbidden light zones[28] which are determined by the critical angle $\theta_c = \pi - \arcsin(1/n_2) \approx 138°$, where n_2 is the reflective index of the substrate.

Discussion

In summary, it has been experimentally demonstrated that cylindrical Si nanoparticles with diameters in the range of 109 to 203 nm and height of 220 nm positioned on a silica substrate have resonant optical responses in the visible spectral range. Theoretical analysis, based on the decomposed discrete dipole approximation, has shown that the optical properties of the Si nanocylinders are determined by their magnetic and electric dipole modes resonantly excited by incident light. With increase of the nanocylinder's diameter the dipole resonances are shifted into the infrared region. The influence of propagation direction and incident light wavelength on the resonant excitation of electric and magnetic modes of Si nanocylinders was considered. The main attention has been given to the case when the the electric and magnetic dipole modes are resonantly excited in the visible spectral range. It has been demonstrated that the total extinction and scattering cross-sections and scattering directivity are strongly dependent on the orientation of Si nanocylinders with respect to the incident direction of light and its polarization. It was found that the directivity of scattered light can be manipulated by the polarization of incident light due to simultaneous resonant excitation of electric and magnetic dipole modes of Si nanocylinders. The demonstrated optical properties of Si nanocylinders can be used for the realization of multi-functional dielectric metasurfaces and optical devices for nanoantenna and sensing applications. Further investigations will be concentrated on optical properties of Si nanocylinders based on resonant excitation of their higher-order multipole modes.
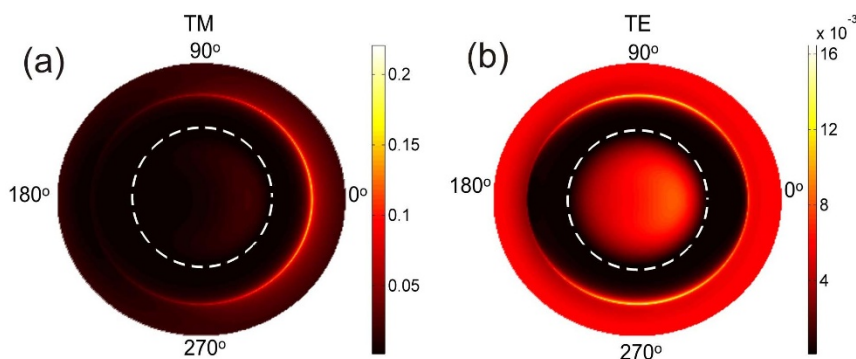
Methods

Figure 8 | Scattering directivity (a.u.) presented in spherical coordinates calculated for the system presented in Fig. 3: a Si nanocylinder with height of 220 nm and diameter of 100 nm is irradiated by a light plane wave with wavelength of 590 nm, the incident angle is 65 degrees. The polar angle $\theta \in [0, \pi]$ is represented by the radial distance, whereas the azimuthal angle $\varphi \in [0; 2\pi]$ is displayed in the figure plane. The center of the circle $\theta = 0$ corresponds to the normal scattering above substrate; the boundary of the circle $\theta = \pi$ corresponds to the normal scattering into substrate. Scattering above (below) the substrate corresponds to the region inside (outside) the white dash circles corresponding to $\theta = \pi/2$. (a) *TM*-polarized incident light, (b) *TE*-polarized incident light.
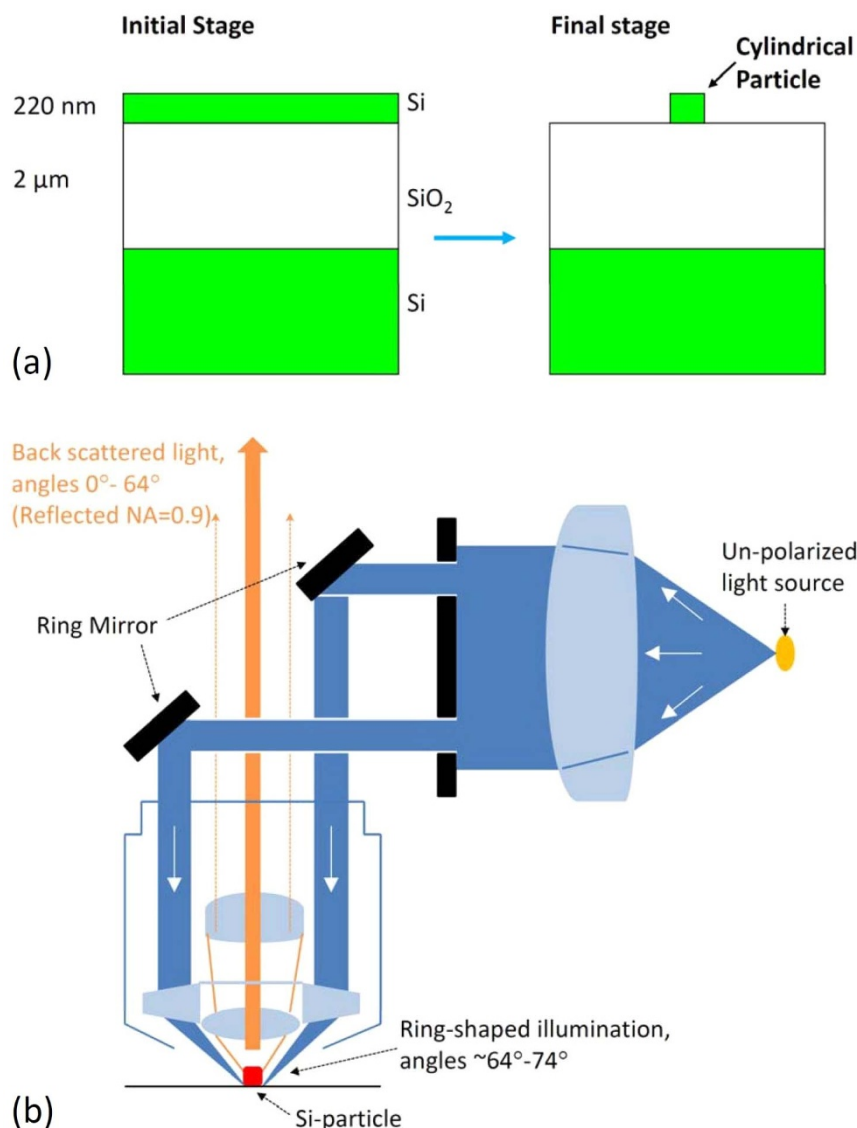
Figure 9 | (a) Schematic presentation of the fabrication stages: initial stage shows a SOI sample before the lithography procedure; final stage shows a Si nanocylinder located on SiO$_2$ substrate. (b) Schematic presentation of the setup for spectroscopic measurements.

subsequent inductively coupled plasma etching on a Soitec SOI wafer with a 220 nm thick Si layer on 2 μm buried oxide. The fabrication is schematically shown in Fig. 9a.

Scattering spectra of the fabricated Si nanocylinders were measured using optical dark-field spectroscopy. The spectroscopic set-up (Fig 9b) included a BX51 microscope (Olympus) equipped with a halogen light source and a fibre-coupled grating spectrometer QE65000 (Ocean Optics). In these measurements a single Si nanoparticle is irradiated at highly oblique angles around 70 deg. and back scattered light collected from angles up to 64 deg. determined by the numerical aperture (NA) of the x100 microscope objective MPLFLNBDP (Olympus). The microscope images were captured with a XC30 digital color camera (Olympus).

Theoretical and numerical methods. For theoretical analysis, we calculated the extinction and scattering cross-sections of cylindrical Si nanoparticles located on a silica substrate using the method of decomposed discrete dipole approximation (DDDA). This method combines the ordinary discrete dipole approximation[29–31] with calculations of cartesian multipole moments of electric dipole systems[15] and their contributions into the extinction and scattering cross-sections. Details of this method can be found elsewhere[15,21]. Briefly, the scattering object is replaced by a cubic lattice of electric point dipoles with a polarizability α_j[32]. The corresponding dipole moment $\mathbf{p}_j$ induced in each lattice point j (with the radius-vector $\mathbf{r}_j$) is found by solving coupled-dipole equations. After solution of these equations, the induced polarization $\mathbf{P}(\mathbf{r})$ of the scatterer can be written as

$$\mathbf{P}(\mathbf{r}) = \sum_{j=1}^{N} \mathbf{p}_j \delta(\mathbf{r}-\mathbf{r}_j). \tag{1}$$

Here $\delta(\mathbf{r}-\mathbf{r}_j)$ is the Dirac delta function. Application of the multipole decomposition[21] to the polarization (1) allows to write

$$\mathbf{P}(\mathbf{r}) \simeq \mathbf{p}\delta(\mathbf{r}-\mathbf{r}_0) - \frac{1}{6}\hat{Q}\nabla\delta(\mathbf{r}-\mathbf{r}_0) + \frac{i}{\omega}[\nabla \times \mathbf{m}\delta(\mathbf{r}-\mathbf{r}_0)]$$
$$+ \frac{1}{6}\hat{O}(\nabla\nabla\delta(\mathbf{r}-\mathbf{r}_0)) - \frac{i}{2\omega}[\nabla \times \hat{M}\nabla\delta(\mathbf{r}-\mathbf{r}_0)]. \tag{2}$$

Here the polarization $\mathbf{P}$ is presented as a sum of multipole terms corresponding to point multipole moments (electric dipole moment $\mathbf{p}$, electric quadrupole moment $\hat{Q}(\mathbf{r}_0)$, magnetic dipole moment $\mathbf{m}(\mathbf{r}_0)$, magnetic quadrupole moment $\hat{M}(\mathbf{r}_0)$, and electric octupole moment $\hat{O}(\mathbf{r}_0)$) located at a point $\mathbf{r}_0$. It is convenient to choose the point $\mathbf{r}_0$ at the scatterer's center of mass[15]. Here we take into account only several first multipole terms considering small scatterers compared to the wavelength. The point multipole moments of the scattering object are simply calculated from the space distribution of $\mathbf{p}_j$[15,21]

$$\mathbf{p} = \sum_{j=1}^{N} \mathbf{P}_j; \quad \hat{Q}(\mathbf{r}_0) = \sum_{j=1}^{N} \hat{Q}^j(\mathbf{r}_0); \quad \mathbf{m}(\mathbf{r}_0) = \sum_{j=1}^{N} \mathbf{m}_j(\mathbf{r}_0);$$
$$\hat{M}(\mathbf{r}_0) = \sum_{j=1}^{N} \hat{M}^j(\mathbf{r}_0); \quad \hat{O}(\mathbf{r}_0) = \sum_{j=1}^{N} \hat{O}^j(\mathbf{r}_0), \tag{3}$$

where the corresponding point multipole moments, associated with the single electric dipole $\mathbf{p}_j$, are under the sum symbols. Analytical expressions for these multipole moments are presented in Ref. 21. Finally, the multipole decomposition (2) is used for calculations of the extinction and scattering cross-sections, as it is shown in Ref. 21.

1. Bohren, C. F. & Huffman, D. R. *Absorption and Scattering of Light by Small Particles* (Wiley, Interscience, New York, 1983).
2. Zhao, Q., Zhou, J., Zhang, F. & Lippens, D. Mie resonance-based dielectric metamaterials. *Mater. Today* **12**, 60–69 (2009).
3. Ginn, J. C. *et al.* Realizing Optical Magnetism from Dielectric Metamaterials. *Phys. Rev. Lett.* **108**, 097402 (2012).
4. Evlyukhin, A. B., Reinhardt, C., Seidel, A., Luk'yanchuk, B. S. & Chichkov, B. N. Optical response features of Si-nanoparticle arrays. *Phys. Rev. B* **82**, 045404 (2010).
5. Garcia-Etxarri, A. *et al.* Strong magnetic response of submicron silicon particles in the infrared. *Opt. Express* **19**, 4815–4826 (2011).
6. Xifré-Pérez, E., Fenollosa, R. & Meseguer, F. Low order modes in microcavities based on silicon colloids. *Opt. Express* **19**, 3455–3463 (2011).
7. Evlyukhin, A. B. *et al.* Demonstration of magnetic dipole resonances of dielectric nanospheres in the visible region. *Nano Lett.* **12**, 3749 (2012).
8. Kuznetsov, A. I., Miroshnichenko, A. E., Fu, Y. H., Zhang, J. & Luk'yanchuk, B. Magnetic light. *Sci. Rep.* **2**, 492 (2012).
9. Shi, L., Tuzer, T. U., Fenollosa, R. & Meseguer, F. A new dielectric metamaterial building block with a strong magnetic response in the sub-1.5-micrometer region: silicon colloid nanocavities. *Adv. Mater.* **24**, 5934–5938 (2012).
10. Krasnok, A. E., Miroshnichenko, A. E., Belov, P. A. & Kivshar, Y. S. All-dielectric optical nanoantennas. *Opt. Express* **20**, 20599 (2012).
11. Rolly, B., Stout, B. & Bonod, N. Boosting the directivity of optical antennas with magnetic and electric dipolar resonant particles. *Opt. Express* **20**, 20376 (2012).
12. Schmidt, M. K. *et al.* Dielectric antennas - a suitable platform for controlling magnetic dipolar emission. *Opt. Express* **18**, 13636–13650 (2012).
13. Zhang, J., MacDonald, K. F. & Zheludev, N. I. Near-infrared trapped mode magnetic resonance in an all-dielectric metamaterial. *Opt. Express* **21**, 26721–26728 (2013).
14. Shi, L. *et al.* Monodisperse silicon nanocavities and photonic crystals with magnetic response in the optical region. *Nature Commun.* **4**, 1904 (2013).
15. Evlyukhin, A. B., Reinhardt, C. & Chichkov, B. N. Multipole light scattering by nonspherical nanoparticles in the discrete dipole approximation. *Phys. Rev. B* **84**, 235429 (2011).
16. Staude, I. *et al.* Tailoring directional scattering through magnetic and electric resonances in subwavelength silicon nanodisks. *ACS Nano* **7**, 7824–7832 (2013).
17. Spinelli, P., Verschuuren, M. A. & Polman, A. Broadband omnidirectional antireflection coating based on subwavelength surface Mie resonators. *Nat. Commun.* **3**, 692 (2012).
18. Van de Groep, J. & Polman, A. Designing dielectric resonators on substrates: Combining plane and electric resonances. *Opt. Express* **21**, 26285–26302 (2013).
19. Zou, L. *et al.* Dielectric resonator nanoantennas at visible frequencies. *Opt. Express* **21**, 1344–1352 (2013).
20. Bezares, F. J. *et al.* Mie resonance-enhanced light absorption in periodic silicon nanopillar arrays. *Opt. Express* **21**, 27587–27601 (2013).
21. Evlyukhin, A. B., Reinhardt, C., Evlyukhin, E. & Chichkov, B. N. Multipole analysis of light scattering by arbitrary-shaped nanoparticles on a plane surface. *J. Opt. Soc. Am. B* **30**, 2589–2598 (2013).
22. Palik, E. *Handbook of Optical Constant of Solids* (Academic, San Diego, CA, 1985).
23. Søndergaard, T. & Bozhevolnyi, S. I. Vectorial model for multiple scattering by surface nanoparticles via surface polariton-to-polariton interactions. *Phys. Rev. B* **67**, 165405 (2003).
24. Kerker, M., Wang, D.-S. & Giles, C. L. Electromagnetic scattering by magnetic spheres. *J. Opt. Soc. Am.* **73**, 765–767 (1983).
25. Fu, Y. H., Kuznetsov, A. I., Miroshnichenko, A. E., Yu, Y. F. & Lukyanchuk, B. Directional visible light scattering by silicon nanoparticles. *Nature Commun.* **4**, 1527 (2013).
26. Person, S. *et al.* Demonstration of zero optical backscattering from single nanoparticles. *Nano Lett.* **13**, 1806–1809 (2013).
27. Evlyukhin, A. B. *et al.* Detuned electrical dipoles for plasmonic sensing. *Nano Lett.* **10**, 4571–4577 (2010).
28. Novotny, L. & Hecht, B. *Principles of Nano-Optics* (Cambridge University, New York, 2006).
29. Draine, B. T. The discrete-dipole approximation and its application to interstellar graphite grains. *Astrophys. J.* **333**, 848 (1988).
30. Draine, B. T. & Flatau, P. J. Discrete dipole approximation for scattering calculations. *J. Opt. Soc. Am. A* **11**, 1491 (1994).
31. Yurkin, M. A. & Hoekstra, A. G. The discrete dipole approximation: an overview and recent developments. *J. Quant. Spectr. Rad. Trans.* **106**, 558 (2007).
32. Evlyukhin, A. B. *et al.* Influence of metal doping on optical properties of Si nanoparticles. *Opt. Commun.* **316**, 56–60 (2014).

Acknowledgments

Author contributions

A.P., S.P. and M.E. fabricated the samples. W.C. and C.R. performed the SEM characterization of the samples. R.L.E., J.B. and S.I.B. performed the optical measurements. A.B.E. worked out the theoretical model, did the numerical calculations. All authors participated in discussion of the results. A.B.E. and B.N.C. wrote the manuscript based on input from all authors. A.B.E. and S.I.B. coordinated the work.

Additional information